1. Introduction

Additive manufacturing (AM), or 3D printing, includes versatile platforms and has become a powerful technology for future advanced manufacturing (1,2). The terms AM, rapid prototyping, and 3D printing are frequently used synonymously. Rapid prototyping (RP) for model making has driven the emergence of 3D printing since the 1980s. A typical 3D printing process involves preprinting, printing, and postprinting. In preprinting, a target object is first transformed into digital data utilizing 3D scanning or a computer-aided design (CAD) model. The CAD model is then sliced into layered data or toolpaths, which will be further fed into an AM machine (or 3D printer). During the printing process, the sequentially layered data (or toolpath) guides the manufacturing of the model or product through ink/material deposition and selective curing. The computer-controlled translation stage precisely moves based on the layered data or toolpath to fabricate objects in a layer-by-layer manner until the completion of the whole construct. The obtained parts (or green parts) are processed in the postprinting to remove support structures, improve surface finishing, or conduct postcuring as needed (Fig. 1).

There is a growing consensus that AM systems have several advantages, including fabrication of intricate geometry with high precision, saving materials, flexibility in design, as well as personalization and customization over traditional techniques (3). In recent years, AM has produced significant scientific and technological impacts and attracted tremendous attention in both academia and industry owing to the above unique features. This trend can be graphically shown by tracing the yearly number of scientific publications from 1990 to 2021 using the terms 'additive manufacturing', 'rapid prototyping,' and '3D printing' (Fig. 2), which exhibited a soaring rise after 2013. This is possibly due to the expiration of the first AM patent, leading to tremendous efforts in AM. The fast-growing trend of AM is expected to continue steadily in the future. Interestingly, publications on 'rapid prototyping' have fallen behind and decreased after 2017, reflecting the fact that the role of AM is gradually shifting from simple prototyping to the next generation of advanced manufacturing. Besides the rapid increase in research, the overall market for AM also shows significant growth rates. The global AM market size was valued at 13.84 billion USD in 2021 and is expected to expand at a compound annual growth rate of 20.8% from 2022 to 2030 (4). The booming research and development in AM are empowered by the enormous industrial application demands, including healthcare, automotive, aerospace, defense, and so on.

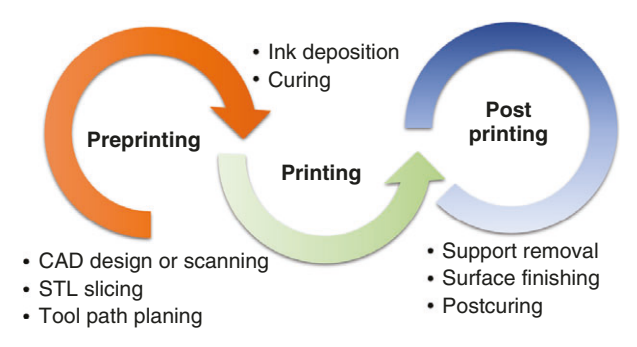


Fig. 1. A typical process of 3D printing: preprinting, printing, and postprinting.

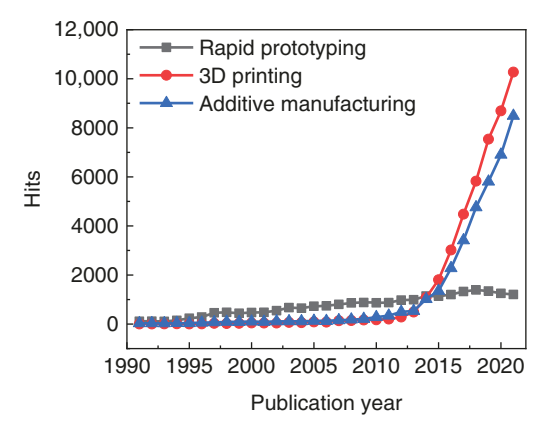


Fig. 2. Yearly number of publications showing the research interest in rapid prototyping, 3D printing, and AM. Data from Web of Science, accessed April 2022.

During the past 40 years, various AM techniques have been developed to fabricate various materials via different mechanisms. Depending on how raw materials are processed into products, AM techniques are classified into seven groups by the International Organization for Standardization (ISO Technical Committee 261) and American Society for Testing and Materials (ASTM) International (Committee F42): binder jetting, directed energy deposition, material extrusion, material jetting, powder bed fusion, sheet lamination, and vat photopolymerization. Each AM technique has advantages and disadvantages in terms of printing resolution, build size, and cost, offering diverse choices for users (Table 1). A wide range of materials, including metals, polymers, ceramics, and concrete, have been successfully printed using different techniques (5–7). As the polymer is the most widely used material, we mainly deal with AM techniques for polymeric materials in this paper. Polymers are long-chain organic molecules with very high molecular weight. Based on their heat processibility, polymers are divided into thermoplastics and thermosets. Thermoplastics are made of linear or branched chain polymers, which can melt upon excess heating and be reshaped and remolded. In contrast, thermosets contain stable polymer networks after initial forming and cannot be melted by heat. Thermoplastics include a variety

Table 1. Classification of AM Techniques According to the ASTM and Their Major Features and Typical Vendors

Technique	Material	Advantage	Disadvantage	Representative 3D printer
Material extrusion (FFF, DIW) Material jetting (inkjet printing, aerosol jetting)	Thermoplastics, thermosets Polymers, wax	Low cost, large size, high versatility Fast printing, multimaterial	Low resolution, slow printing High cost, low viscosity inks	MakerBot, RepRap Dow chemical 3D systems, Stratasys
Binder jetting	Thermoplastics, foundry sand	Fast printing, large size	Limited materials	ExOne, Voxeljet
Powder bed fusion (SLS, SLM, MJF)	Polymers and metals	High resolution, high quality	Expensive, formation of pores	EOS, 3D systems, HP, Desktop Metal
Vat polymerization (SLA, DLP, TPP)	Photopolymers (acrylates, epoxides)	Fast printing, high resolution	Limited materials	3D systems, ObJet
Sheet lamination (LOM)	Paper, metals	Low cost, large size	Inferior surface quality, simple shape	Fabrissonic
Directed energy deposition Metals, foundry	Metals, foundry	Accurate composition, excellent properties	Low accuracy	Optomec, POM

of semi-crystalline polymers and amorphous polymers that can be reprocessed multiple times after material synthesis, making them suitable for heat-based AM. Thermosets are formed through a curing or cross-linking process whereby polymerization occurs between small-molecule monomers and cross-linkers. Heat and light are widely used stimuli to trigger thermosets curing. Among them, thermal-curable resins use heat as the trigger for cross-linking, which is usually a slow process. In contrast, photo-sensitive resins (or photopolymers) can be cured by light, such as Ultraviolet (UV) light, for rapid photopolymerization. These UV-curable resins possess fast cross-linking capabilities and are suitable for light-based AM techniques.

Here, we provide a comprehensive summary of the fundamentals of AM techniques for polymers. The printing process, working mechanism, and material systems for various polymer AM techniques are elaborated. Additionally, the advantages and disadvantages of each technique are summarized. We also briefly discuss some other fast-growing AM techniques, including hybrid printing, volumetric printing, and bioprinting. Lastly, the future development and trend in AM in terms of printing techniques, materials, and design/modeling methods are highlighted.

2. Additive Manufacturing Methods and Materials

2.1. Material Extrusion

2.1.1. Techniques. The extrusion-based AM refers to the techniques that use computer-controlled deposition of molten or semi-molten polymers, pastes, polymer solutions, or dispersions through a movable nozzle or extrusion printhead in a line-by-line then layer-by-layer manner. In this approach, inks/materials are first extruded through a nozzle with the aid of a mechanical force. Then, the deposited material filaments undergo solidification through physical transition (such as crystallization and physical gelation) or chemical cross-linking. After printing one layer, the extrusion head either moves up or the build platform moves down to make space for depositing material for the next layer. This process is repeated until the printing is finished. Extrusion-based AM mainly includes the techniques of fused filament fabrication (FFF; or fused deposition modeling, FDM), and direct ink writing (DIW; or direct write, DW; or robot casting).

FFF is the most commonly used AM technique due to its low cost and wide accessibility. Crump invented and trademarked FDM in 1989 and shortly founded the company Stratasys (Rehovot, Israel) (8). Whilst FFF is the official term for this method according to the ISO and ASTM, its equivalent term, FDM (trademarked by Stratasys), is also commonly used. In the FFF process, a solid thermoplastic (or its composite) filament is fed through a heated nozzle as the feedstock, which is converted into a semi-molten state, followed by deposition on the building platform (Fig. 3). The hot polymer filaments solidify rapidly because of cooling below their glass transition temperature or crystallization temperature by the environment and the print bed. Note that the print bed in FFF is typically heated to a temperature lower than the transition temperature to slow down the cooling and reduce the residual stress. The diffusion of polymer chains at the filament interfaces enables the bonding of adjacent polymer filaments. Several printing

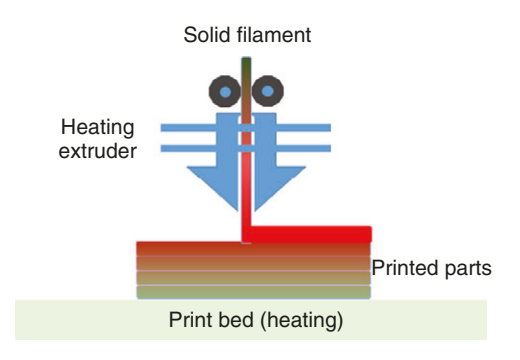


Fig. 3. Schematic and process of FFF printing.

parameters, such as the extrusion temperature, feed/deposition rate, print bed temperature, and so on, are critical to the successful printing, which includes near net shape and strong interlayer bonding of deposited filaments (9). The printing resolution for FFF usually falls on the order of a few hundreds of microns.

DIW works similarly to FFF but uses viscous inks to create structures with controlled architecture and composition (10). A viscous ink with the shear thinning effect flows through a small nozzle by a piston, air pressure, or a screw at modest shear rates and forms a nonflowable filament with high viscosity after dispensing (Fig. 4). After deposition, some curing processes (e.g., photopolymerization and thermal curing) are required to solidify the printed structures. Pseudoplastic inks with shear thinning features are necessary for successful DIW printing. To accommodate the printing of target inks/materials, the rheological properties should be optimized and evaluated before printing. Oftentimes, rheological modifiers of nanoparticles, such as fumed silica or nanoclay, are added to tune the viscosity. In some cases, rheological modifiers are not preferred in low-viscosity inks, which are normally difficult to print by DIW. This problem can be overcome by the following approaches. First, use printheads coupled with additional in situ curing devices (e.g., UV lamps or heating elements) (11). Second, print sacrificial materials as the support to protect the weak materials (12). Lastly, perform embedded printing using a self-healing fugitive support bath (13).

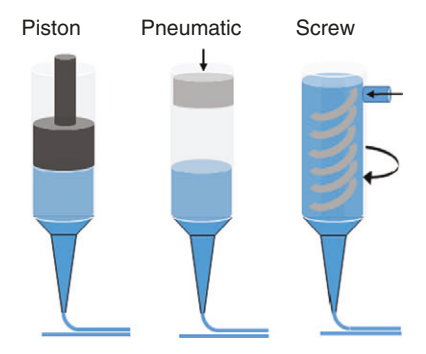


Fig. 4. Schematic and process of DIW printing.

Because of the development of these approaches, DIW has nearly no restrictions on ink composition and has gained great popularity in recent years.

Driven by the need to fabricate heterogeneous functional structures and devices, multimaterial extrusion printing has been actively explored. The direct approach to multimaterial extrusion is the use of multiple nozzle extruders. For example, spatially controlled thermoplastic deposition in the same printing job was realized by the multiple extrusion nozzles (14). Microfluidics extrusion (15), micromixer-based co-extrusion (16), and coaxial extrusion (17) have also been exploited for extrusion-based multimaterial printing. Recently, a multimaterial multinozzle DIW printing approach was reported to realize high-resolution, high-speed multimaterial printing (18). Additionally, multimaterial DIW printing was achieved using photo-thermal dual-cure resins (19).

Big-area additive manufacturing (BAAM), which was originally developed by Cincinnati Incorporated (Harrison, OH, USA) and Oak Ridge National Laboratory's Manufacturing Demonstration Facility, is a large-scale FFF system (20). It uses a large nozzle (~10 mm) to increase material deposition rate and a large gantry system for large structures, such as car bodies, mobile houses, bridges, or boat hulls (21), which are significantly larger than typical FFF build platforms (typical dimensions of ~300 mm by 300 mm).

2.1.2. Materials

2.1.2.1. Thermoplastics. FFF is widely used to print engineering thermoplastics. It uses filaments of solid thermoplastics and composites as the feedstock, which are heated above their melting temperature for extrusion and then rapidly solidified upon cooling. The filaments are processed by mixing the thermoplastic matrix, pigment, reinforcements, and other additives using single or twin-screw extruders. A wide range of engineering thermoplastic polymers, including polylactic acid (PLA) (22), acrylonitrile butadiene styrene (ABS) (23), high-impact polystyrene, thermoplastic polyurethane (TPU) (24), polycarbonate (PC) (25), polyamide (or Nylon) (26,27), polyether ether ketone (PEEK) (28), and polyetherimide (PEI) (29) have been used to fabricate filaments with different properties. Among them, PLA and ABS are the most widely used ones. PLA is a biodegradable, bio-based green plastic with excellent mechanical properties. ABS, consisting of acrylonitrile blends and copolymers, butadiene-containing polymers, and styrene, is another prevalent material showing high toughness and impact resistance. TPU is a common engineering elastomer for FFF with a break strain of up to 600% (24). PEEK and PEI are two high-performance engineering plastics with melting temperatures over 340°C and tensile moduli over 2 GPa (29-31). In addition, particles, such as clay, metal oxides, carbon nanotubes, and short fibers, including chopped carbon fibers, and other natural polymer fibers, are blended with the different thermoplastics to create thermoplastic composite filaments with enhanced properties for FFF printing. More recently, continuous carbon fiber reinforced composites were printed by FFF using a customized nozzle and filament supply system (32). The detailed mechanical properties of these typical engineering plastics printed by FFF are listed in Table 2.

Thermosets and composites are normally printed by DIW using liquid precursors and proper rheological modifiers. For example, tough interpenetrating polymer network (IPN) epoxy was printed by using a hybrid ink containing photocurable acrylates and thermal-curable epoxy and fumed silica by UV-assisted

7

Table 2. Common Filaments and Major Physical Properties for FFF

Materials	Reinforcement	Tensile strength (MPa)	Young's modulus (MPa)	Fracture strain (%)	Glass transition temperature/ melting temp- erature (°C)	References
PLA	_	26–64	1100-1500	3–7	62/167	(22)
	2 wt% talc	51 - 57	1300 - 1500	6.5 - 7.3	61/174	
	5 wt% CF	30 – 32	900-1100	10 - 13	61/167	
ABS	_	17 - 34	1900-2400	2.0 - 8.6	113	(23)
	$5 \text{ wt}\% \text{ TiO}_2$	17 - 33	1500	1.6 - 3.8	_	
	$5 \text{ wt}\% \text{ Al}_2 ilde{ ext{O}}_3$	12 - 29	_	1.6-2.9	_	
	5% Jute fiber	9-24	_	1.6 – 4.2	_	
	5% SEBS	8-25	_	1.9 - 3.6	_	
TPU	_	19-29	12	450 – 600	200	(24)
	2% MWCNT	25	25	600	200	
PA1012	_	24 - 27	320 - 440	100 - 300	177	(26)
PA12	_	40 - 44	1430-1490	20 – 68	178	(27)
	6 wt% GNP	37 - 41	2010-2200	6-12	178	
PC	_	36 - 53	2100-2400	2.0 - 4.3	145	(25)
PP	_	19-21	900-930	8	167 - 168	(33)
	12 μm glass spheres	18–22	1290–1770	3–5	166	
PEEK		79–84	2400	6 - 17	143/343	(28,31)
PEI	_	68–79	200	4–7	210–215/ 340–400	(29)

DIW printing (34). The modulus and glass transition of the epoxy composite can be widely tuned by altering the ratio of the photocurable and thermal-curable components. Light-weight cellular epoxy composites were printed by adding silicon carbide whiskers, carbon fibers, and nanoclay into epoxy resin (35). Polydicyclopentadiene-based thermosets and composites were printed by DIW printing via heat-triggered frontal polymerization (36).

Elastomers and composites have also been printed by DIW printing. Aliphatic urethane diacrylate was formulated with *n*-butyl acrylate diluent and fumed silica rheological modifier composites inks for UV-assisted DIW printing (37). Semi-crystalline polycaprolactone (PCL) was also added to form a semi-interpenetrating polymer network, showing highly enhanced mechanical properties and shape memory effect. Polydimethylsiloxane (PDMS) and its composites with customizable material properties and other functional properties have been printed by DIW printing. Fillers, including carbon nanotubes (CNT), boron nitride, and magnetic particles, can be added into PDMS composite inks for printing functional materials and devices (38). For example, hard magnetic particles (such as NdFeB) were mixed with PDMS and fumed silica to print magnetoactive soft materials with a programmed magnetization domain for actuators (39,40). Thermosetting silicone can be printed without any support structures by the simultaneous control of both reaction kinetics and transient rheology (41).

DIW printing of hydrogels is extensively studied for biomedical applications (42–44). For example, bilayered structures consisting of a thermoresponsive

hydrogel and nonthermoresponsive hydrogels, such as polyacrylamide, were printed by dual-nozzle DIW printing to realize controlled and complex shape changes (42,45). Extrusion-based bioprinting of hydrogels with good biocompatibility and biodegradability is widely studied for drug delivery and tissue engineering (46).

Other functional polymers, such as liquid crystal elastomers (LCEs), have been used for DIW printing (47–50). Extrusion-induced shearing enables effective LCE mesogen alignment, which is necessary for LCE actuation. Therefore, DIW printing is the major technique for LCE printing. To do so, a viscous LCE ink was first synthesized by LCE oligomers and chain extenders, such as n-butylamine, using a base catalyst (47). Then, the viscous ink was extruded at an elevated temperature below the nematic to its isotropic transition temperature $T_{\rm NI}$ and subsequently cross-linked by UV light to lock the mesogen alignment. The molecular alignment could be locally programmed by controlling the printing path, thereby enabling complex shape-changing, which finds broad applications in soft robots and actuators (47,49,50–53). Additionally, some conductive polymers such as poly(3,4-ethylene dioxythiophene): polystyrene sulfonate) (PEDOT: PSS) have been printed by DIW printing for bioelectronics applications (54).

2.1.3. Summary. Both FFF and DIW have some prominent advantages over other printing techniques, including low cost, low complexity, and high flexibility. They can use low-price feedstock materials. FFF printers with a price as low as a few hundred dollars can offer good printing quality. Various filament materials with different properties are widely available in the market. Therefore, FFF has become the most used AM technique. However, it exhibits low build speed, low resolution, and poor surface quality (100-300 µm). FFF-printed parts typically possess a large residual stress due to the temperature gradient. These parts also suffer from weak and anisotropic mechanical properties compared to their injection molding counterpart due to weak interlayer bonds and voids formed by filament-based layer-wise manufacturing. This issue is more critical when printing different materials with poor material compatibility. Different strategies, including annealing, optimizing printing parameters, postprocessing, and feedstock chemical modification, have been used to enhance the polymer sintering and inter-filament bonding (55). It should be mentioned that another reason for FFF's popularity is that it prints engineering thermoplastics. However, this also limits its capability to print high-performance thermosets.

DIW printing, as a more versatile printing platform, provides a complement to FFF. DIW is suitable for printing a wide range of materials, including thermoplastics, thermosets, hydrogels, LCE, and other functional materials (such as conductive inks). Therefore, DIW can be regarded as the most versatile printing technique in terms of the selection of printing materials and is one of the most popular AM techniques in academic research. However, the major drawbacks of DIW are its low build speed and low resolution (also for FFF). Some recent work show that by using a very fine nozzle, the printing resolution can go to several microns but the printing speed drops significantly. The printing speed can be improved by multinozzle extrusion printing (18).

2.2. Material Jetting

2.2.1. Techniques. Material jetting is an AM process that uses selectively deposited material droplets to form the target entity. It covers the techniques

of inkjet printing (IJP) and aerosol jet printing (AJP). IJP usually uses rows of piezoelectric nozzles with sizes on the order of 20–40 µm to deposit ink drops as the printhead travels across the build plate (Fig. 5) (56). A complete layer of the target structure can be rapidly created by a few quick passes of the printhead. As most of the inks used in IJP are photo-sensitive resins, a few passes of UV light can cure each newly deposited layer rapidly. Particularly, the PolyJet technique developed by Stratasys is an advanced form of IJP that enables high-resolution digital printing of multimaterials. It can offer a high resolution of 600 dpi in the x-y build plane. The layer thickness can go to 16–32 µm depending on the quality mode (57). To create complex structures, both the building material and the support material are deposited and cured. Moreover, PolyJet allows the creation of the so-called digital materials, that is, a set of materials whose properties (glass transition temperature and stiffness) can be digitalized within a specific range. To do so, more than one building material inks (typically one rigid and one soft) are deposited side-by-side in a predetermined ratio that determines the final macroscopic properties of the printed part (58).

AJP, or maskless mesoscale materials deposition (M3D), was developed by Optomec Inc. (Albuquerque, NM, USA) and commercialized in 2004 for printing electronics (59). The droplet jetting is realized by the atomization of the building material in the aerosol chamber by ultrasonification (1.6–2.4 MHz) or pneumatic atomization. To realize successful jetting, the viscosity of the materials usually should not exceed 2500 mPa·s, and the dispersed particles possess a sufficiently small diameter to avoid clogging. The building material stream is focused and accelerated through a nozzle with an internal diameter of 50-300 µm, and dense aerosol with droplet diameters of 1-5 µm can be obtained. The high lateral resolution focus of the particle stream is maintained by a high-speed annular sheath gas stream (10–100 m/s) within the deposition head. Consequently, a high building speed of up to 200 mm/s can be achieved. It should be noted that although AJP is a jetting method, its feedstock and printing path are similar to those of DIW and therefore share the major advantages and disadvantages of DIW. Additionally, AJP machines are significantly more expensive than DIW hardware. Therefore, AJP still finds more applications in printing electronics.

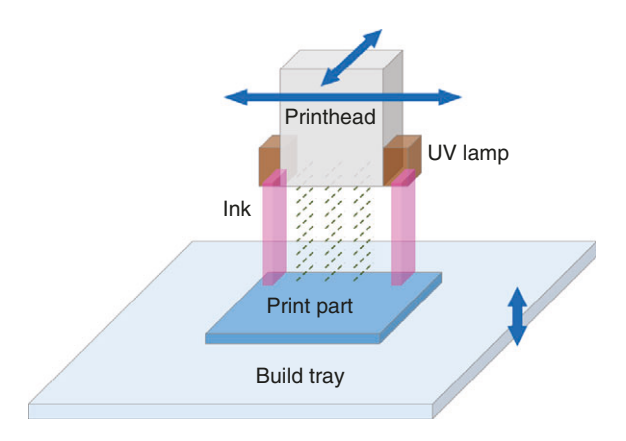


Fig. 5. Schematic and process of IJP.

2.2.2. Materials. IJP AM requires both building materials and support materials with low viscosity (such as 20 cp) in the printhead for jetting. The resin for IJP is usually heated to reduce its viscosity, but the heating temperature is typically limited to below ~70°C because of the temperature limit of piezo actuators used for jetting. Therefore, resins for inkjet AM should have excellent thermal stability and fast UV cure capability. Commercial resin inks consist of acrylic oligomer/monomers, surfactants, photo initiators, and other additives. The support material developed by Stratasys was based on water-soluble monomers and polymers, and photocuring gives an intentionally weak material so that it be removed with water. Instead, 3D Systems (Rock Hill, SC, USA) uses wax as the support material, which can be removed by mild heating.

Materials for AJP have some requirements on their parameters such as the viscosity and maximum particle size to enable a successful atomizing and printing process (60). AJP's high resolution makes it suitable to print functional materials and devices. Particularly, electronic structures, including conducting tracks, thin film transistors, and conductive or semi-conductive structures, are printed using inorganic or metal particle-based inks. Conductive and semi-conductive polymers such as PEDOT: PSS blends can also be printed (61).

2.2.3. Summary. IJP prints a layer by a few passes of the printhead and thus enables high build speed. Polyjet printing also allows 3D multimaterial or multicolor structures to be built with different optical or mechanical property gradients in one printing job, which is a significant advantage over other printing techniques. In conventional IJP, the resolution is always limited to tens or hundreds of microns, which is reduced to ~400 µm for digital material printing. Compared with IJP, AJP has a higher lateral resolution of up to 10 µm, and layer thicknesses of 100 nm can be reached. However, the use of concentrated polymer solutions or solutions that contain filler particles leads to material clogging, limiting the variety of printable materials in AJP. Similarly, IJP has a stringent requirement on the ink properties, such as low viscosity (<20 cP), limiting its ability to use new materials, such as customized materials or functional materials. For this reason, the research in material development for IJP is very limited. IJP also requires a completely dense support structure, making it less effective and less economical to print porous and lattice structures than other AM techniques. It is also noted that the high equipment cost of Polyjet, as well as AJP, is another barrier for their wide applications in materials research.

2.3. Binder Jetting

2.3.1. Techniques. Binder Jetting (BJ) is a type of AM process that utilizes the deposition of liquid binding agents onto a powder bed to join powder particles and form 3D objects. With the selection of an appropriate liquid binder, BJ can be used to process virtually any powder materials. BJ was first invented at the Massachusetts Institute of Technology (MIT) in the early 1990s (62) and subsequently licensed to several companies such as ZCorp (acquired by 3D Systems), ExOne (North Huntingdon, PA, USA), and VoxelJet (Friedberg, Germany). The schematic of the BJ process is shown in Figure 6. In the BJ process, a layer of fresh powder feedstock is spread over the print bed, and a liquid binder is jetted onto selected regions of the print bed through overhead printhead nozzles to join the wetted powder particles. Thereafter, a fresh layer of powder is spread on top of the previous layer, and the process repeats itself until the 3D object is constructed.

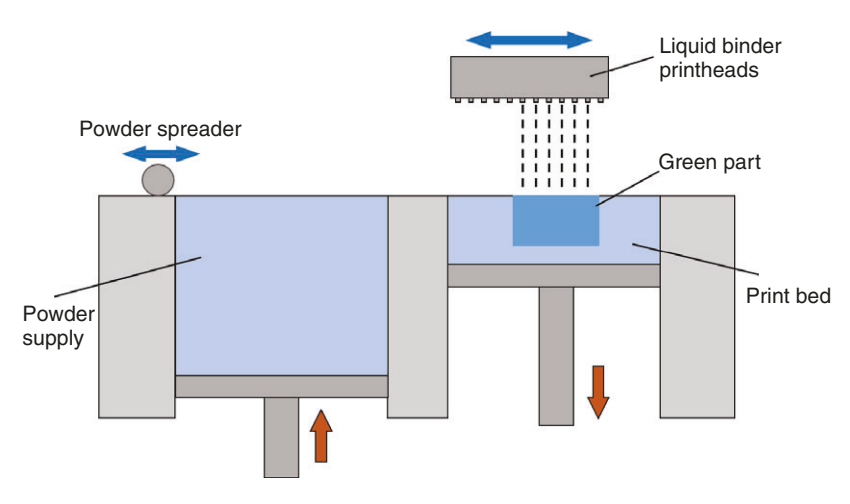


Fig. 6. Schematic and process of BJ printing.

The build is subsequently removed from the printer and then undergoes a curing process before the individual parts can be extracted. The cured part, also known as the 'green' part, will often be subjected to further postprocessing such as high temperature sintering or infiltration to improve its mechanical properties.

- 2.3.2. Materials. Despite its ability to process any powder material, BJ is rarely used to produce polymer parts because the as-printed 'green' parts have high porosity and require additional sintering to achieve higher densification. As polymers have relatively low melting temperatures as compared to metals and ceramics, they are more suitable to be processed by other AM methods like powder bed fusion (PBF) to efficiently produce dense parts without the need for additional postprocessing. However, polymer BJ printing can be used for certain applications where a porous structure is required. For example, polymer powders such as PLA, PCL, polyglycolic acid (PGA), and polyethylene oxide (PEO) have been fabricated using BJ for drug delivery and biomedical scaffolding applications (63–65). Voxel-Jet also offers a commercial poly-methyl methacrylate (PMMA) powder that can be used for casting applications (66).
- 2.3.3. Summary. BJ possesses a higher build rate than material jetting processes as it only dispenses the liquid binder, which makes up only a small portion of the total part volume. Additionally, BJ printers have large build volumes which allow for the fabrication of multiple parts. For instance, BJ printers are used for sand casting applications where parts can be continuously printed without a limitation in length (67). In BJ, the unused powder acts as a support structure for the printed parts and can be reused indefinitely because of the lack of heating elements. The customizability of the liquid binder enables more freedom in materials design, allowing for BJ to fabricate multicolored parts and functionally graded materials. Although BJ has a high build rate, the as-printed 'green' parts are highly porous, resulting in low mechanical properties that do not satisfy the industrial standards for certain structural components. Additional post-processing such as sintering and infiltration will be required for BJ to produce functional components, resulting in a significant increase in the fabrication time and cost.

2.4. Powder Bed Fusion

2.4.1. Techniques. PBF is an AM process that utilizes one or more heat sources to selectively fuse powders to fabricate parts. PBF is highly versatile and can be used to fabricate a wide variety of materials, including polymers, metals, ceramics, and composites. Moreover, PBF is capable of fabricating industrial-grade parts and is used in the automotive and aerospace industries for direct manufacturing. Selective laser sintering (SLS) and multi jet fusion (MJF) are the leading polymer PBF techniques that are widely used in industrial applications to date.

SLS is a mature industrial polymer PBF technique that was first developed at the University of Texas and later patented in 1990 (68). The schematic of an SLS printer is shown in Figure 7. SLS employs a CO_2 laser as its heat source to selectively fuse regions of the powder layer in a point-wise scanning approach. Fresh powder layers are evenly distributed onto the print bed using a powder spreading mechanism. The SLS printing process is performed inside a build chamber with an inert atmosphere (typically nitrogen-filled) to reduce the laser-induced oxidation of the material (69). Prior to the printing process, powder feedstock is preheated to a stable temperature close to the material melting point to reduce the laser energy required to achieve particle fusion. Additionally, part warpage caused by nonuniform part crystallization is prevented by maintaining an elevated build chamber temperature.

Since the commercialization of the first SLS printer in 1992, many new variations of SLS printers have been developed. While the fusion mechanism remains the same, several components in SLS, such as the laser type, number of lasers, powder spreading mechanism, and build volume have been modified to improve the printing speed, printing resolution, and part quality. Fine detail resolution (FDR) is a variation of SLS developed by the equipment manufacturer EOS (Krailling, Germany) that utilizes an ultra-fine CO₂ laser beam to

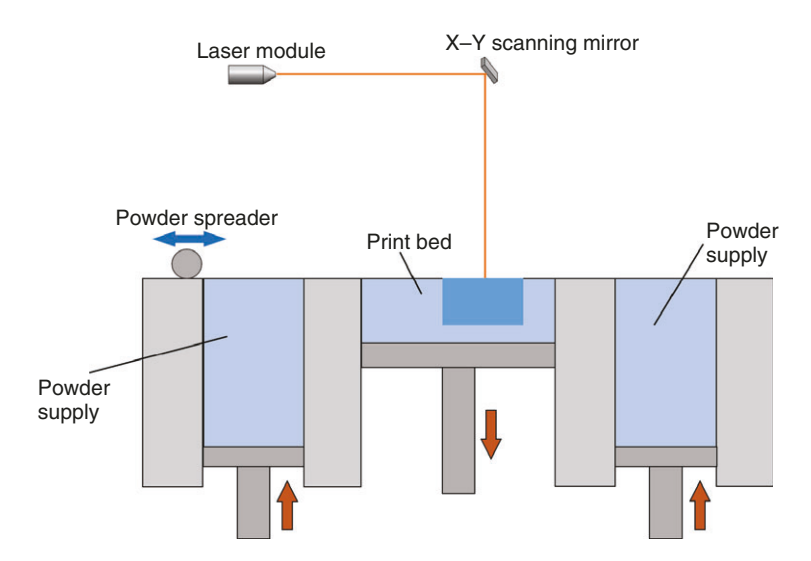


Fig. 7. Schematic and process of SLS printing.

produce polymer parts with extremely fine resolution surfaces. LaserProFusion technology is an upcoming SLS solution by EOS that is equipped with up to 1 million diode lasers, which can be activated simultaneously to fuse an entire powder layer to achieve significantly higher printing speeds. Farsoon's Flight® Technology (Changsha, China) is another variation of SLS that features the use of high-power fiber lasers and a novel scanning system to provide higher part resolution and faster printing speeds.

MJF is an innovative PBF technology commercialized in 2016 by HP Inc. (Palo Alto, CA, USA) (70). The MJF printing process features a combination of PBF and binder jetting where a proprietary fusing ink agent is jetted from overhead printhead nozzles onto the powder layer to facilitate powder fusion (Fig. 8). The fusing ink agent, consisting of radiation-absorbing materials, is deposited onto selective regions of the powder layer to raise the local heat absorption of the wetted particles. After the deposition of the fusing agent, the entire powder bed is heated by an array of overhead infrared (IR) lamps in an area-wide pass, and only the powder particles wetted with the fusing agent will absorb sufficient heat to coalesce and fuse together. In addition to the fusing agent, a water-based detailing agent is simultaneously dispensed along the contour of the printed part to prevent the adherence of surrounding powder and improve part resolution.

With its area-wise fusion approach, MJF can achieve printing speeds that are 10 times faster than SLS (71). The usage of IR lamps also removed the need for an inert environment, which significantly reduces the preparation time and operation cost. Through its multiagent jetting capability, MJF offers another degree of freedom in material design and can even fabricate multicolored parts.

2.4.2. Materials. Thermoplastic polymer powders are most used in PBF printing because of their high compatibility with PBF processes (Table 3). Firstly, thermoplastic materials have relatively low melting points and can be fabricated without excessive energy consumption. Secondly, thermoplastic materials also possess low thermal conductivities which prevent the occurrence of thermal bleeding, a phenomenon where unwanted powder particles adhere to or fuse with

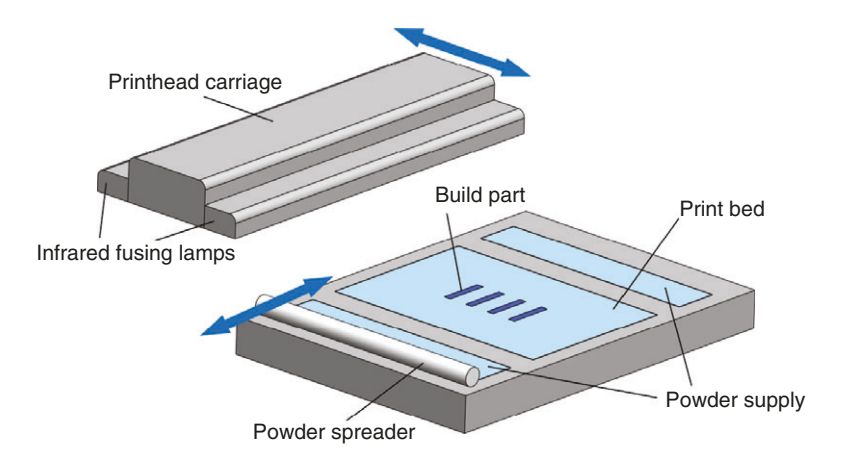


Fig. 8. Schematic and process of MJF printing.

Table 3. Commercial Polymer Powders Used for PBF Techniques

Material	Compatible PBF techniques	Material features	Manufacturer
PA12	SLS, MJF	Good mechanical strength Chemically resistant	EOS, 3D Systems, Arkema, Prodways, BASF, HP
PA11	SLS, MJF	 High mechanical strength Chemically resistant Impact resistant	EOS, 3D Systems, Arkema, Prodways, BASF, HP
Polyamide 6 (PA6)	SLS	 High mechanical strength and stiffness Excellent thermal stability	BASF
TPU	SLS, MJF	Excellent flexibility and toughnessAbrasion resistant	EOS, 3D Systems, Prodways, BASF
Polypropylene (PP)	SLS, MJF	 Good mechanical strength Chemically resistant	EOS, Prodways, BASF
Polystyrene (PS) SLS	 High stiffness Low impact resistance	EOS, 3D Systems
PolyEther- KetoneKetone (PEKK)	SLS	 Excellent mechanical strength Excellent thermal and chemical resistance Flame retardant 	Arkema

the printed object. Lastly, thermoplastic powders have high recyclability, which contributes to the high-cost effectiveness of PBF processes.

Thermoplastic polymers can be further categorized into amorphous and semicrystalline thermoplastics. Amorphous thermoplastics have randomly arranged molecular structures while semicrystalline thermoplastics consist of a combination of crystalline and amorphous structures. While both amorphous and semicrystalline thermoplastics are processable using PBF, amorphous thermoplastics such as polystyrene (PS) have limited commercial applications because they typically possess a broad melting range, resulting in the nonuniform melting of particles during the PBF printing process. The nonuniform melting and cooling of particles create printing defects like porosity, which negatively impacts the part quality. However, the fabrication of porous amorphous thermoplastics is suitable for casting applications where porosity is beneficial to expedite the melting process (72,73).

In contrast, semicrystalline thermoplastics possess sharper melting points, resulting in more consistent melting and consolidation of particles during the printing process. The intrinsic thermal properties of semicrystalline thermoplastics enable the fabrication of highly dense parts with excellent mechanical properties. Among the semicrystalline thermoplastics, polyamides such as polyamide 12 (PA12) and polyamide 11 (PA11) are the most widely used materials in PBF due to their large sintering window, which is defined as the difference between the onset melting temperature and onset crystallization temperature of the material. The large sintering window of polyamides enables them to be processed over wider temperature ranges without any part distortion or warpage (74). PA12 and PA11 powders are commercially available for both SLS and MJF, while other thermoplastic materials, such as high-performance polymers, polyesters, and so on, are only commercially available for SLS. Table 3 provides an overview of thermoplastic powders that are commercially available in SLS and MJF and the major companies that manufacture them. These commercial powders are widely used in the aerospace and automotive industries to fabricate functional components for replacing existing machine parts. In addition to the commercial powders, the fabrication of biocompatible polymers using PBF has been an active area of research to expand PBF applications into the biomedical industry. Biocompatible polyesters such as PCL and PLA are commonly fabricated via SLS for the development of bone tissue engineering applications (75–77).

Polymer composites are produced through the addition of inorganic fillers to the polymer matrix with the goal of improving targeted material properties such as mechanical performance, stiffness, and thermal stability. As AM applications gradually shift from rapid prototyping toward end-use manufacturing, the development of composite materials is essential to further expand the industrial applications of AM. In polymer PBF processes, commercially available composite powders are currently limited to polymers reinforced with microfillers because the cost to effectively prepare composite powders with good nanofiller dispersion is extremely high. The commercially available composite powders mostly comprise of glass-filled and fiber-reinforced polyamides, as shown in Table 4. As MJF is a relatively new PBF technique, there is only one composite powder commercially available. However, there are several research

Table 4. Composite Polymer Powders Used for PBF Techniques

PBF technique	Base material	Filler	Manufacturer/reference
SLS	PA12	Glass beads	EOS, 3D Systems
		Aluminum particles	EOS, 3D Systems
		Mineral fibers	3D Systems
		Glass beads and carbon fibers	EOS
	PA11	Glass beads	Prodways, BASF
		Carbon black	Prodways
		Carbon fibers	EOS, BASF
	PA6	Mineral reinforcement embedded in PA6 particles	BASF
	PEKK	Carbon fibers	EOS
MJF	PA12	Glass beads	HP
		Aramid fibers	(78)
		Glass fibers	(79)

studies dedicated to the development of MJF composites. Chen and co-workers (78) successfully developed an aramid fiber-reinforced PA12 composite with exceptional mechanical properties using MJF. Liu and co-workers (79) demonstrated the effect of high temperature annealing on the mechanical performance of glass fiber-reinforced PA12 composites printed using MJF.

Thermoset polymers generally possess better thermal, mechanical, and chemical properties than thermoplastics due to the chemical cross-linking that occurs during the curing process. However, the fabrication of thermoset polymers using PBF is extremely challenging. In recent years, several breakthroughs have been made in the manufacture of thermoset polymers using SLS. The materials manufacturer Tiger (Jonesboro, GA, USA) has launched the Tigital[®] series of thermoset powders for SLS, which can be printed at a low process temperature of 75°C with low part shrinkage and warpage. The printed thermoset parts were then subjected to a postprint curing process in an oven to complete the cross-linking process. Campbell and co-workers (80) adopted an alternative method to fabricate thermoset-based epoxy resin by partially curing the material prior to the SLS printing. Hassan and co-workers (81) successfully fabricated carbon-reinforced Bismaleimide powder using a multistage postcuring process after SLS printing.

2.4.3. Summary. In PBF, multiple parts of different geometries can be arranged freely within the build unit to effectively utilize the build space. With the development of new PBF techniques like MJF and LaserProFusion, the printing speeds of PBF continue to improve and have the potential to compete with traditional manufacturing methods like injection molding. Parts printed by PBF can be readily used after bead blasting and do not require additional postprint processes such as infiltration or heat treatment. Additionally, PBF processes do not require the fabrication of additional support structures as the unfused powder in the build is used to support the printed parts. Unfused powder in the build can also be recycled and used for subsequent prints, leading to a reduction in the material cost and wastage.

PBF-printed parts are susceptible to the formation of internal pores, resulting in an adverse effect on the mechanical properties of the printed part. Porosity is a prevalent printing defect that could be attributed to several factors such as poor powder packing and the lack of fusion between adjacent powders or layers. PBF materials must also possess specific optical and thermal properties to be processable. For instance, SLS materials must be capable to absorb radiation at the wavelength of the laser source, and MJF powders must be of a light color to prevent excessive thermal bleeding during the IR exposure. These, in general, limit the types of materials that are suitable for PBF.

2.5. Vat Photopolymerization

2.5.1. Techniques. Vat photopolymerization (VP)-based printing techniques use photopolymerizable liquid inks to solidify materials selectively. A laser beam or a UV light can be used as the light source to induce the photocuring, which is called stereolithography (SLA, when a laser beam is used) and digital light processing (DLP, when a projector is used), respectively. Based on the direction of light irradiation, both bottom-up and top-down approaches are used for VP-based printing. Table 5 summarizes vat photopolymerization-based techniques.

	•	• •	• •
Techniques	Light sources	Printing features	Manufacturer/reference
SLA DLP CLIP TPP HARP	320–360 nm laser 385–405 nm LED 385–405 nm LED 780–800 nm laser 385–405 nm LED	Low speed, good precision High speed, good precision High speed, good precision Low speed, nano resolution High speed, large area	3D systems, Formlabs 3D systems, EnvisionTec Carbon 3D Nanoscribe Azul

Table 5. Summary and Features of Vat Photopolymerization Printing Techniques

SLA is one of the earliest methods of AM, which was developed in the 1980s. The term 'stereolithography' (SLA) was coined by Hull in an early patent, which laid the groundwork for commercial AM and later the company 3D Systems (82). In a typical top-down SLA printing process, a fast-scanning laser beam (usually in the UV range) with a small spot size (~10 µm) is used for selective solidification (Fig. 9). After curing one layer, the platform moves down to replenish ink on the top of the previous layer for curing. Here, the top layer goes down, giving the name top-down. As the ink renewal is a time-consuming step, the ink viscosity plays a critical role in the speed of SLA printing (83). The vertical resolution, which is the smallest possible layer thickness, mainly depends on the light penetration depth into the material and the resulting curing depth, and therefore the light dose and photo absorbance. Light absorbing additives, such as organic dyes, nanoparticles, and pigments, are effective in attenuating the light and thus improve the z resolution. After printing, a posttreatment process such as heating or photocuring is frequently used for printed parts to achieve the desired mechanical performance and surface finish.

DLP printing utilizes photo masks to selectively solidify a photo-sensitive resin and build the part in a layer-by-layer fashion. The development of DLP-based 3D printing stems from the image projection technique developed by Hornbeck in Texas Instruments (Dallas, TX, USA) in the 1980s (84). The core part is the light modulator, a digital micro-mirror device (DMD) that contains millions of digitally controllable micron-sized mirrors. With the light-emitting diodes (LEDs) as the light source, a DMD allows the generation of binary dynamic photo patterns (black and white images) and reflects on the resin vat by a mirror

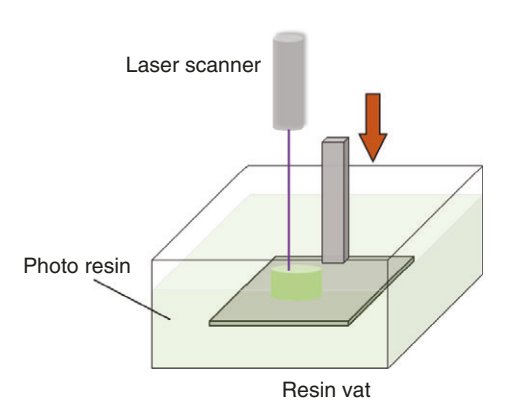


Fig. 9. Schematic and process of SLA printing.

to trigger the photocuring. Liquid crystal displays (LCDs) have also been used as digitally modulated light sources for a similar task. In a typical bottom-up DLP printing, the light source is positioned below the resin vat and is directed upward to the transparent window made of a low-adhesion material (such as TEFLON or PDMS) (Fig. 10). The first layer of the part is cured and adheres firmly to the build stage surface. The build stage moves up and separates from the vat window, and the subsequent layers are cured onto the previous layers. This process is repeated until the 3D object is printed. Here, the bottom layer of the printed part moves up, giving the name bottom-up. The mirror size in a DMD device is about 5–7 μm. An optical lens magnifies or reduces the size. Therefore, the resolution of the DLP-based 3D printing can range from 2-3 µm to 100-200 µm, with 50-100 µm being the most often used. High resolution (micro- and nanoscale) DLP can be achieved by using proper optical lens systems (called projection micro-stereolithography, PµSL) (85–87). The use of a digital light source also enables the modulation of the grayscale light pattern for grayscale-DLP printing to achieve multimaterial- (88,89) or multicolor-like printing (90).

Continuous liquid interface production (CLIP) is a variant of DLP printing, which further enhances the printing speed and is among the fastest 3D printing techniques that are suitable for large-scale industrial production (87,91). CLIP exploits an oxygen-permeable film to inhibit photopolymerization (or dead-zone) near the vat window, allowing continuous build stage elevation without the need for separation between the printed layer and the window. Consequently, continuous pulling-out of the cured parts at the speed of 500 mm per hour was realized (87). CLIP has been commercialized by the company Carbon 3D (Redwood City, CA, USA).

High-area rapid printing (HARP) is a stereolithographic AM technique using a mobile liquid interface (such as a fluorinated oil) to reduce the reaction heat accumulation of the adhesive forces between the interface and the printed object for large-area printing. Owing to the effective heat dissipation of flowing oil, direct cooling across the entire print area is realized. Consequently, continuous vertical print rates exceeding 430 mm per hour with a volumetric throughput of 100 liters per hour were achieved (92). Lattice structures made from hard plastics, ceramic precursors, and elastomers can be printed. HARP is commercialized by the company Azul (Skokie, IL, USA).

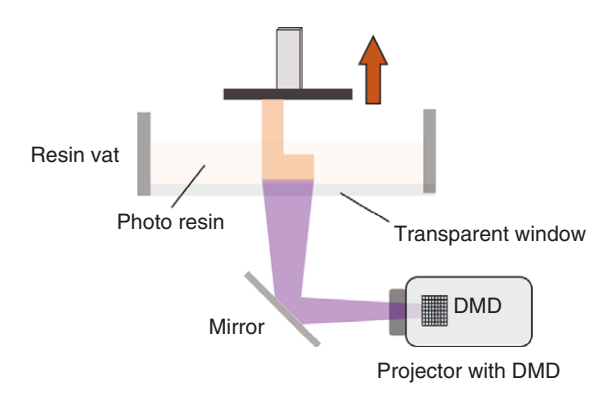


Fig. 10. Schematic and process of DLP printing.

Direct laser printing via two-photon polymerization (TPP) has been utilized for nano- and submicron-scale structure printing (93–95). TPP has been used to induce polymerization for a long time. Since the emergence of more powerful lasers and more sensitive photo resin systems, TPP has been explored as a lithographic technique in the 1990s (96). For this technique, a focused laser with high photon density is used to trigger two-photon polymerization via two-photon absorption and subsequent polymerization (Fig. 11). Usually, NIR lasers (such as Ti: sapphire laser with a wavelength of 780 nm) are used for TPP to reduce the light scattering and improve the penetration depth. Curing of the photo-sensitive resin is achieved by adjusting the light intensity beyond a polymerization/fabrication threshold, and the light intensity also defines the voxel size of the curing. The typical spatial resolution built by TPP is below 100 nm. The feature resolution may be further reduced to less than 65 nm with the addition of radical quenchers or light inhibitors (97). TPP AM is commercialized by Nanoscribe GmbH &Co (Karlsruhe, Germany).

Because only one vat of resin is used, vat photopolymerization was generally regarded as unsuitable for multimaterial AM. In recent years, efforts have been undertaken to print multimaterial-like structures using DLP, such as using switchable vats (98), selective wavelength curing (99), or microfluidics vat (100). Among the developed techniques, single vat grayscale light (88) appears to be promising and can achieve almost continuous modulus variation ranging from ~1 MPa to ~1 GPa within a single layer. Recently, this technique has been further developed to print multicolored parts (90).

2.5.2. Materials. The typical components of the ink for vat photopolymerization include photo-active resins and initiators. Other important components include diluents, radical inhibitors, and light absorbers. The diluents can reduce the liquid viscosity to accelerate the ink renewal process. The radical inhibitors, such as methoxy hydroquinone, can increase the gelation threshold of acrylates to reduce overcuring. The light absorbers can attenuate the light and suppress the scattering light restrain to reduce the penetration depth so as to enhance the printing resolution (101). The photo-cross linking reactions are classified as radical systems, cationic systems, and hybrid (dual-cure; or two-stage cure) systems. (Meth)acrylates and (meth)acrylamides are the most commonly employed monomers for free radical photopolymerization due to their rapid reaction rates and low cost. Benzoyl-based photo-initiators, such as I651 and I184, require UV (A or B) light sources suitable for SLA using UV laser (320–360 nm). Acyl

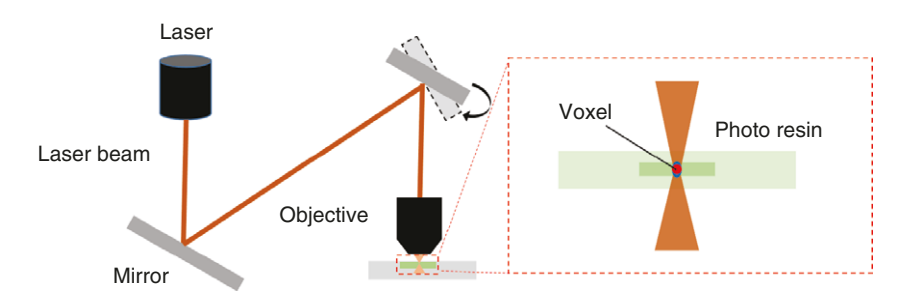


Fig. 11. Schematic and process of TPP printing.

phosphine oxide photo-initiators, such as phenyl bis(2,4,6-trimethyl benzoyl) phosphine oxide (I819), are more preferred for DLP printing using a higher wavelength projector (385–405 nm).

Liquid acrylate and methacrylate are the major components of photo resin for VP-based printing. Most of the resin contains some content of multifunctional acrylates, such as trimethylol propane trimethacrylate, pentaerythritol tetraacrylate (PETA), 1,6-hexanediol diacrylate, bisphenol A diglycidyl ether as cross linkers, and monofunctional acrylate, such as *iso*-bornyl acrylate, as a reactive diluent. It is noted that the polymerization of acrylates usually induces volume shrinkage, leading to some residual stress in the printed parts (101). The use of bulky structured oligomers, such as cycloaliphatic diacrylate, or other high-molecular oligomers can reduce the volume shrinkage.

Thiol-ene-based formulations are another radical-based photo resin for VP printing. It exhibits reduced shrinkage volume and residual stress relative to acrylate-based formulations due to the delay of the gel point. As the thiol-ene networks are formed by step-growth kinetics, more homogenous networks with lower cross-linking density are formed in the structure (102). Therefore, thiol-ene polymers, usually less brittleness with enhanced toughness, have been developed. Thiol-ene-based super stretchable silicone elastomers (break strain up to 1400%) have been printed by DLP (103).

Epoxides are one of the most used classes of monomers for photo-based SLA through chain-growth cationic-curing mechanisms. Epoxides can undergo significantly less shrinkage (2–3% volumetric) than acrylates during photo-cross-linking (104). Epoxy monomers, including diglycidyl ether derivatives of bisphenol A, 3,4-epoxycyclohexyl-methyl-3,4-epoxycyclohexanecarboxylate, and trimethyloyl propane, are widely used. As pure epoxide cures much slower than acrylates, other more reactive cationic polymerizable monomers, including vinyl ether monomer and oxetanes, can be used (104).

The use of multiple types of hybrid monomers with different reaction mechanisms and reaction rates has become popular. The hybrid formulations containing both radical and cationic monomers and initiators have been long studied (105). The cured IPN provides better mechanical properties and less volume shrinkage compared with a single acrylate-based network (106). More recently, photo-thermal dual-cure systems containing photocurable acrylates and thermally curable thermosets have been studied for DLP printing (107–109). The photocuring of the acrylate component holds the shape during printing and provides the essential mechanical properties for the printed green parts. After printing, a post thermal curing step can initiate the cross-linking of thermoset components, such as epoxy resin, to sequentially form IPN with highly enhanced mechanical properties. This method makes many previously unprintable thermosets printable by DLP printing.

Besides chemically cross-linking thermosets and elastomers, semi-crystalline and amorphous thermoplastics have been printed using precursors without cross-linkers. Thiol-ene chemical between 1,6-hexane dithiol and diallyl terephthalate was exploited to print poly(ethylene terephthalate) (PET) by SLA (110). High molecular weight ($>10^4$ g/mol) non-cross-linked PET is formed within less than 5 s of visible light exposure at ambient conditions using low intensities (1-10 mW/cm²). The obtained PET showed excellent mechanical

properties with an ultimate tensile strength of 24 MPa at a failure strain of 800%. Similarly, highly reactive monoacrylate, such as *iso*-bornyl acrylate, and 4-acryloylmorpholine, have been used to print thermoplastics with excellent mechanical properties by DLP printing (111). A thiol chain transfer agent was used to regulate the molecular weight of the thermoplastics. Finally, soluble, meltable, and reprocessable thermoplastics are obtained, which can be used as sacrificial molds.

In addition, particles and short fibers can be added into the photocuring resin for DLP printing. Specifically, high solid loading ink paste were prepared by adding large amounts of ceramic particles, including Al_2O_3 , TiO_2 into a fast curable photopolymer matrix to print composite parts, which transform into ceramic constructs through careful pyrolysis (112). As the composite inks consisting of particles and fibers usually possess high viscosities, mechanical swiping systems are often used in these DLP printers to facilitate resin deposition before cross-linking.

2.5.3. Summary. While SLA prints high-quality parts at a fine resolution as low as 10 µm, it is relatively slow. DLP printing can provide a much higher build speed due to its all-at-once curing manner. The emergence of CLIP printing makes it possible to print parts at an industrial production rate. TPP allows the printing of small-sized constructs at the nanoscale resolution. Usually, TPP is limited to small size and slow fabrication speed. Recently, DMD has been used for TPP, enabling enhanced build speed and scalable size (113,114). The photopolymerization-based printing methods usually display volume shrinkage and thus produce internal stress in printed parts, which influences the printing accuracy and mechanical properties. Proper material selections, optimized printing parameters, and posttreatment are commonly used to mitigate these issues. One of the advantages of light-based printing is the wide choice of light wavelengths, initiators, and monomers to cure materials with widely tunable mechanical properties and other physical properties according to the user's needs (115,116). Moreover, the concept of dual-cure by combining photocuring and thermal curing can significantly expand the material library for light-based printing.

3. Emerging AM Methods

3.1. Hybrid AM. Integrating multiple printing techniques (or hybridizing) can provide or improve spatial control of the material, geometry, and functionality. Early in 2005, commercial SLA machines were combined with DIW for automated and efficient hybrid manufacturing of complex electrical devices (117). Recently, a hybrid printing system consisting of top-down DLP printing and DIW printing for multimaterial AM was reported (118). The DLP module enables high-resolution, high-speed printing of geometrical-complex structures, and the DIW printing module enables printing of functional materials such as LCEs and conductive silver ink. Multimaterial, multimethod (m⁴) AM platforms were also developed by integrating four different printing modules (IJP, FFF, DIW, and AJP), robotic arms for pick-and-place (PnP), as well as an intense pulsed light (IPL) sintering system (119). With these platforms, complex structures and functional devices, including actuators, soft robotics and electronics, can be readily printed in a single printing job.

3.2. 4D Printing. Since 2013, four-dimensional (4D) printing has attracted tremendous interest (120-123). It was initially defined as '3D printing + time', where the fourth dimension is time. Currently, 4D printing is widely defined as that the shape, property, and functionality of 3D-printed structures would change with time under the predetermined stimulus after printing. In 4D printing, stimuli-responsive smart materials and proper structural design are usually used for 3D printing of shape programmable structures. The on-demand shape and property changes after printing enable several prominent advantages: (1) direct fabrication of intelligent devices with on-demand shape-shifting capability; (2) saving printing time and materials for thin-walled structures or lattice structures; (3) saving space for storage and transportation because of the stimuli-triggered shape-changing. For example, self-folding can accelerate the fast prototyping of 3D objects by saving 60-87% of both the printing time and material consumption (124,125). Therefore, 4D printing has become a fast-growing research field in various disciplines, such as smart material and advanced manufacturing. 4D printing enables the on-demand complex geometry and stimuli-responsive capability of printed parts, thereby finding applications in various fields, including actuators, soft robots, active metamaterials, smart electronics, self-folding structures, biomedical devices, and tissue engineering (126-129).

3.3. Other Printing Techniques. Volumetric printing has been developed to allow for the printing of constructs within seconds to minutes. Using this technique, the entire 3D object is simultaneously created by irradiating a volume of photo-sensitive resin from multiple angles, as opposed to the conventional layer-by-layer process. Currently, three different approaches are used to realize volumetric printing. In its first conceptualization, a system architecture comprises of mirrors that divide a single light beam into three orthogonal beams, projecting a holographic figure into a photo-sensitive resin to fabricate the desired objects (130). The superposition of multiple beams coming from fixed, predetermined orientations can usually print simple objects. The second approach is tomographic reconstruction, which enables the production of more complex objects by using two-dimensional (2D) dynamic light fields. Inspired by computed tomography, a series of 2D light patterns, computed by the Radon transform, is projected synchronously into a rotating resin container with optically transparent and viscous photo resins (131). Through the superposition of multiple 2D images of the same object viewed at different angles, the desired 3D structure in centimeter scale with a resolution of up to 80 μm can be fabricated in a single step (132). More recently, xolography-based linear volumetric printing was developed to activate printing constructs as large as 30 mm (133). The central idea is to use dual-color photo-switchable photo-initiators to induce local polymerization inside a confined monomer volume upon linear excitation of resin by intersecting light beams.

Bioprinting is an AM technique used to print tissue constructs using bioinks. It provides a robust approach to fabricating customized constructs to match patients' unique anatomical structures as personalized 3D representations of tissues, thereby finding broad applications in drug delivery, tissue engineering, and regenerative medicine (134,135). A major feature of the 3D bioprinting technique is the use of 'bioinks' composed of extracellular matrix (ECM)-like support biomaterials, living cells, and/or other bioactive components

23

to print 3D tissue constructs (136,137). A prerequisite of the bioinks is their compatibility with supporting embedded living cells. Biomaterial hydrogels with a high-water-content environment similar to the physical properties of the native ECM are extensively used for bioprinting (138,139). Various printing modalities, including extrusion-based (46), light-based (116), and inkjet printing (140), have been exploited for the bioprinting of cell tissues with intricate shapes, relevant cell types, and desired biofunctions for diverse applications.

4. Outlook

AM has experienced rapid advancement during the past decade and has continued to reshape the advanced manufacturing field as a game-changing technology. It revolutionizes manufacturing from conventional centralization to distributed fabrication and from mass production to customized fabrication. With the wide adoption of AM techniques, future developments in the field may include the following aspects:

The AM techniques require robust control over geometry and material composition at multiple scales. The native materials usually display the hierarchy in multiple scales to realize extreme mechanical properties and unique functions (141). Therefore, biomimetic AM is a topic of great interest (142,143). To achieve that, various multimaterial printing techniques and external field-assisted printing methods have been developed to realize the control over the material composition, mechanical property gradient, and microscale alignment of the powder particles (88,144–146). Despite these advances, the conflict between the printing size and resolution of conventional techniques still blocks further control over the composition and hierarchical architectures. Therefore, chemical and physical techniques, including self-assembly and external fields, can be exploited to manipulate the sophisticated structures.

In terms of materials, more eco-friendly (such as bio-based and biodegradable materials) and other functional materials (as well as their composites) should be developed for different printing techniques. With the prevailing concept of carbon peak and carbon neutralization, material sustainability should be considered in material development. Although AM is regarded as a more sustainable manufacturing technique, there is still a large amount of solid plastic being disposed of at the end of the product lifetime, leading to resource waste and environmental pollution. The use of biodegradable and bio-based PLA has been a positive development so far. Down the road, the use of renewable materials, such as lignin and cellulose, as feedstock or additives to fabricate materials for printing can enhance sustainability (147,148). Besides, particle- and fiber-reinforced composite materials and inks should be developed for 3D printing. 3D printing of composites is ideal for moldless rapid prototyping and fabrication of materials with enhanced mechanical properties for engineering applications. Additionally, novel inks/materials containing liable bonds or dynamic chemical bonds can be used to print covalent adaptive polymers or vitrimers, enabling on-demand recycling and degradability of the printed materials (149). The development of functional inks for 3D printing of multifunctional materials, including shape memory polymer, LCE, hydrogels, and magnetoactive materials, can greatly expand its applications

in diverse fields in 4D printing, including tissue engineering, biomedical devices, and aerospace (150).

Lastly, advanced design and control software are needed to further empower AM techniques at different stages. Before printing, simulation/modeling provides a robust method to guide the design of structures with unprecedented properties. For example, machine learning has been used to design multimaterials structures for highly improved toughness (151). The extended finite element method combined with density-based topology optimization was used for multimaterial design optimization (152). Simulation/modeling also provides a low-cost and efficient approach to understanding the multiphysics during printing, such as reaction-diffusion coupling and thermal-mechanical coupling, thereby optimizing the printing parameters (101,153,154). Machine vision-assisted machine learning has been used to print on the fly (155). After printing, modeling/simulation is valuable to predict the shape change in 4D printing. For example, evolutionary algorithms have been successfully used to predict the multimaterial design of active composites with complex shape actuations (156–158). Most of the existing modeling processes are research-based customized methods that require tremendous knowledge in mechanics and design to use. In the future, more versatile and robust software should be developed to satisfy the needs of users from different disciplines.

In summary, AM has become a disruptive force in next-generation advanced manufacturing. Many printing techniques, materials systems, and design methods have been developed to make AM faster, smarter, and more robust. Multidisciplinary efforts also usually push the development of AM. With the advancement in materials, hardware, and software, AM continues to reshape the field of manufacturing and promises to contribute to the fourth industrial revolution.

Acknowledgments

HJQ and XK acknowledge the support of the grants from the US Air Force Office of Scientific Research (FA9550-19-1-0151 and FA9550-20-1-0306), US Office Naval Research (N00014-21-1-2258), US National Science Foundation Industry—University Cooperative Research Center (IUCRC) SHAP3D (Science of Heterogeneous Additive Printing of 3D Materials) (IIP-1822141), and the gift funds from Northrop Grumman Corporation, and HP Inc. KZ and WS acknowledge the support of the Singapore RIE2020 Industry Alignment Fund — Industry Collaboration Projects (IAF-ICP) Funding Initiative, as well as cash and in-kind contribution from the industry partner, HP Inc., through the HP-NTU Digital Manufacturing Corporate Lab.

BIBLIOGRAPHY

- 1. J. W. Stansbury and M. J. Idacavage, Dent. Mater. 32 (1), 54-64 (2016).
- S. H. Huang, P. Liu, A. Mokasdar, and L. Hou, Int. J. Adv. Manuf. Technol. 67 (5), 1191–1203 (2013).
- 3. S. C. Ligon, R. Liska, J. Stampfl, M. Gurr, and R. Mülhaupt, *Chem. Rev.* **117** (15), 10212–10290 (2017).

25

- 4. 3D Printing Market Size, Share & Trends Analysis Report By Component (Hardware, Software, Services). Available from https://www.grandviewresearch.com/industryanalysis/3d-printing-industry-analysis. Cited April, 2022.
- 5. D. Helmer and B. E. Rapp, Nat. Mater. 19 (2), 131–133 (2020).
- 6. Z. C. Eckel, C. Zhou, J. H. Martin, A. J. Jacobsen, W. B. Carter, and T. A. Schaedler, Science 351 (6268), 58-62 (2016).
- 7. W. E. Frazier, J. Mater. Eng. Perform. 23 (6), 1917–1928 (2014).
- 8. S. S. Crump, Apparatus and Method for Creating Three-Dimensional Objects, 1992, Google Patents.
- 9. X. Gao, S. Qi, X. Kuang, Y. Su, J. Li, and D. Wang, Addit. Manuf. 37, 101658 (2020).
- 10. J. A. Lewis, Adv. Funct. Mater. 16 (17), 2193–2204 (2006).
- 11. L. L. Lebel, B. Aissa, M. A. E. Khakani, and D. Therriault, Adv. Mater. 22 (5), 592–596 (2010).
- 12. V. C.-F. Li, X. Kuang, C. M. Hamel, D. Roach, Y. Deng, and H. J. Qi, Addit. Manuf. 28, 14-22 (2019).
- 13. Y. Jin, A. Compaan, W. Chai, and Y. Huang, ACS Appl. Mater. Interfaces 9 (23), 20057-20066 (2017).
- 14. D. Espalin, J. Alberto Ramirez, F. Medina, and R. Wicker, Rapid Prototyp. J. 20 (3), 236-244 (2014).
- 15. W. Liu, Y. S. Zhang, M. A. Heinrich, F. De Ferrari, H. L. Jang, S. M. Bakht, M. M. Alvarez, J. Yang, Y.-C. Li, G. Trujillo-de Santiago, A. K. Miri, K. Zhu, P. Khoshakhlagh, G. Prakash, H. Cheng, X. Guan, Z. Zhong, J. Ju, G. H. Zhu, X. Jin, S. R. Shin, M. R. Dokmeci, and A. Khademhosseini, *Adv. Mater.* **29** (3), 1604630 (2017).
- 16. D. Kokkinis, F. Bouville, and A. R. Studart, Adv. Mater. 30 (19), 1705808 (2018).
- 17. Q. Pi, S. Maharjan, X. Yan, X. Liu, B. Singh, A. M. van Genderen, F. Robledo-Padilla, R. Parra-Saldivar, N. Hu, W. Jia, C. Xu, J. Kang, S. Hassan, H. Cheng, X. Hou, A. Khademhosseini, and Y. S. Zhang, Adv. Mater. 30 (43), 1706913 (2018).
- 18. M. A. Skylar-Scott, J. Mueller, C. W. Visser, and J. A. Lewis, *Nature* 575 (7782), 330-335 (2019).
- 19. W. Li, X. Liu, Z. Deng, Y. Chen, Q. Yu, W. Tang, T. L. Sun, Y. S. Zhang, and K. Yue, Adv. Mater. 31 (48), 1904732 (2019).
- 20. A. Roschli, K. T. Gaul, A. M. Boulger, B. K. Post, P. C. Chesser, L. J. Love, F. Blue, and M. Borish, Addit. Manuf. 25, 275–285 (2019).
- 21. B. K. Post, P. C. Chesser, R. F. Lind, A. Roschli, L. J. Love, K. T. Gaul, M. Sallas, F. Blue, and S. Wu, Virtual Phys. Prototyp. 14 (2), 123–129 (2019).
- 22. X. Gao, D. Zhang, S. Qi, X. Wen, and Y. Su, J. Appl. Polym. Sci. 136 (31), 47824 (2019).
- 23. A. R. Torrado, C. M. Shemelya, J. D. English, Y. Lin, R. B. Wicker, and D. A. Roberson, Addit. Manuf. 6, 16–29 (2015).
- 24. C. Hohimer, N. Aliheidari, C. Mo, and A. Ameli, in Smart Materials, Adaptive Structures and Intelligent Systems, American Society of Mechanical Engineers, 2017.
- 25. M. Domingo-Espin, J. M. Puigoriol-Forcada, A.-A. Garcia-Granada, J. Llumà, S. Borros, and G. Reyes, *Mater. Des.* **83**, 670–677 (2015).
- 26. X. Gao, D. Zhang, X. Wen, S. Qi, Y. Su, and X. Dong, Rapid Prototyp. J. 25 (7), 1145–1154 (2019).
- 27. D. Zhu, Y. Ren, G. Liao, S. Jiang, F. Liu, J. Guo, and G. Xu, J. Appl. Polym. Sci. 134 (39), 45332 (2017).
- 28. K. M. Rahman, T. Letcher, and R. Reese, in ASME International Mechanical Engineering Congress and Exposition, American Society of Mechanical Engineers, 2015.
- 29. V. Schöppner and K. P. KTP, Proceedings of the 69th Annual Technical Conference of the Society of Plastics Engineers (ANTEC'11), Boston, MA, USA, 2011.
- 30. Y. Zhao, K. Zhao, Y. Li, and F. Chen, J. Manuf. Process. 56, 28-42 (2020).
- 31. S. Ding, B. Zou, P. Wang, and H. Ding, Polym. Test. 78, 105948 (2019).

- 32. R. Matsuzaki, M. Ueda, M. Namiki, T.-K. Jeong, H. Asahara, K. Horiguchi, T. Nakamura, A. Todoroki, and Y. Hirano, Sci. Rep. 6, 23058 (2016).
- 33. M. Spoerk, F. Arbeiter, I. Raguž, G. Weingrill, T. Fischinger, G. Traxler, S. Schuschnigg, L. Cardon, and C. Holzer, *Macromol. Mater. Eng.* **303** (7), 1800179 (2018).
- 34. K. Chen, X. Kuang, V. Li, G. Kang, and H. J. Qi, Soft Matter 14 (10), 1879–1886 (2018).
- 35. B. G. Compton and J. A. Lewis, Adv. Mater. 26 (34), 5930–5935 (2014).
- I. D. Robertson, M. Yourdkhani, P. J. Centellas, J. E. Aw, D. G. Ivanoff, E. Goli, E. M. Lloyd, L. M. Dean, N. R. Sottos, P. H. Geubelle, J. S. Moore, and S. R. White, *Nature* 557 (7704), 223–227 (2018).
- 37. X. Kuang, K. Chen, C. K. Dunn, J. Wu, V. C. Li, and H. J. Qi, *ACS Appl. Mater. Interfaces* **10** (8), 7381–7388 (2018).
- M. Saadi, A. Maguire, N. Pottackal, M. S. H. Thakur, M. M. Ikram, A. J. Hart, P. M. Ajayan, and M. M. Rahman, *Adv. Mater.* 2108855 (2022).
- 39. Y. Kim, H. Yuk, R. Zhao, S. A. Chester, and X. Zhao, *Nature* **558** (7709), 274–279 (2018).
- C. P. Ma, S. Wu, Q. J. Ze, X. Kuang, R. D. Zhang, H. J. Qi, and R. K. Zhao, ACS Appl. Mater. Interfaces 13 (11), 12639–12648 (2021).
- 41. W. Stephanie, D. Uranbileg, T. Dylan, B. Callie, Y. O. Dogan, O. Gina, and M. Yigit, 3D Print. Addit. Manuf. 6 (3), 139–147 (2019).
- S. Naficy, R. Gately, R. Gorkin, H. Xin, and G. M. Spinks, *Macromol. Mater. Eng.* 302 (1), 1600212 (2017).
- 43. D. Han, Z. Lu, S. A. Chester, and H. Lee, Sci. Rep. 8 (1), 1963 (2018).
- A. Sydney Gladman, E. A. Matsumoto, R. G. Nuzzo, L. Mahadevan, and J. A. Lewis, Nat. Mater. 15 (4), 413–418 (2016).
- J. Liu, O. Erol, A. Pantula, W. Liu, Z. Jiang, K. Kobayashi, D. Chatterjee, N. Hibino,
 L. H. Romer, and S. H. Kang, ACS Appl. Mater. Interfaces 11 (8), 8492–8498 (2019).
- X. Cui, J. Li, Y. Hartanto, M. Durham, J. Tang, H. Zhang, G. Hooper, K. Lim, and T. Woodfield, Adv. Healthc. Mater. 9 (15), 1901648 (2020).
- C. P. Ambulo, J. J. Burroughs, J. M. Boothby, H. Kim, M. R. Shankar, and T. H. Ware, ACS Appl. Mater. Interfaces 9 (42), 37332–37339 (2017).
- 48. A. Kotikian, R. L. Truby, J. W. Boley, T. J. White, and J. A. Lewis, *Adv. Mater.* **30** (10), 1706164 (2018).
- D. J. Roach, X. Kuang, C. Yuan, K. Chen, and H. J. Qi, Smart Mater. Struct. 27 (12), 125011 (2018).
- D. J. Roach, C. Yuan, X. Kuang, V. C.-F. Li, P. Blake, M. L. Romero, I. Hammel, K. Yu, and H. J. Qi, ACS Appl. Mater. Interfaces 11 (21), 19514–19521 (2019).
- M. O. Saed, C. P. Ambulo, H. Kim, R. De, V. Raval, K. Searles, D. A. Siddiqui, J. M. O. Cue, M. C. Stefan, and M. R. Shankar, *Adv. Funct. Mater.* 29 (3), 1806412 (2019).
- 52. A. Kotikian, C. McMahan, E. C. Davidson, J. M. Muhammad, R. D. Weeks, C. Daraio, and J. A. Lewis, *Sci. Robot.* 4, eaax7044 (2019).
- A. Kotikian, J. M. Morales, A. Lu, J. Mueller, Z. S. Davidson, J. W. Boley, and J. A. Lewis, Adv. Mater. 33 (27), e2101814 (2021).
- H. Yuk, B. Lu, S. Lin, K. Qu, J. Xu, J. Luo, and X. Zhao, Nat. Commun. 11 (1), 1604 (2020).
- 55. A. Andreu, S. Kim, J. Dittus, M. Friedmann, J. Fleischer, and Y.-J. Yoon, *Addit. Manuf.* 55, 102773 (2022).
- 56. B. J. de Gans, P. C. Duineveld, and U. S. Schubert, Adv. Mater. 16 (3), 203-213 (2004).
- 57. M. W. Barclift and C. B. Williams, *International Solid Freeform Fabrication Symposium*, University of Texas at Austin, Austin, Texas, 2012.
- M. Jochen, C. Diana, S. Manuel, S. Ralph, and S. Kristina, 3D Print. Addit. Manuf. 4 (4), 193–199 (2017).
- 59. M. J. Renn, Direct Write System, O.D. Company, Editor, US, 2006.

27

- TOETWENS TON ADDITIVE MANOI ACTORIS
- N.-S. Kim and K. N. Han, J. Appl. Phys. 108 (10), 102801 (2010).
 R. Aga, C. Jordan, R. S. Aga, C. M. Bartsch, and E. M. Heckman, IEEE Electron Device Lett. 35 (11), 1124–1126 (2014).
- E. Sachs, M. Cima, P. Williams, D. Brancazio, and J. Cornie, J. Eng. Ind-T Asme 114 (4), 481–488 (1992).
- 63. B. M. Wu, S. W. Borland, R. A. Giordano, L. G. Cima, E. M. Sachs, and M. J. Cima, J. Control. Release 40 (1-2), 77–87 (1996).
- 64. J.-H. Ahn, J. Kim, G. Han, D. Kim, K.-H. Cheon, H. Lee, H.-E. Kim, Y.-J. Kim, T.-S. Jang, and H.-D. Jung, *Addit. Manuf.* **41**, 101988 (2021).
- 65. M. Ziaee and N. B. Crane, Addit. Manuf. 28, 781-801 (2019).
- 66. VoxelJet, Binder Jetting 3D Printing & Binder Jetting Printers, 2022. Available from https://www.voxeljet.com/additive-manufacturing/3d-printing-processes/binderjetting-technology/. Cited February 24, 2022.
- 67. C. Sutcliffe, Apparatus For Manufacturing Three Dimensional Items, U.S.P. Office, Editor., The University of Liverpool, 2008.
- 68. J. J. Beaman and C.R. D'eckard, Selective Laser Sintering with Assisted Powder Handling, U.S.P. Office, Editor. 1989, The University of Texas System.
- 69. M. Schmid, A. Amado, and K. Wegener, J. Mater. Res. 29 (17), 1824–1832 (2014).
- 70. HP, HP Multi Jet Fusion Technology, in Technical White Paper, 2017. Available from https://reinvent.hp.com/us-en-3dprint-wp-technical.
- Z. Y. Xu, Y. Wang, D. D. Wu, K. P. Ananth, and J. M. Bai, J. Manuf. Process. 47, 419–426 (2019).
- 72. M. Chhabra and R. Singh, Rapid Prototyp. J. 17 (5), 328–350 (2011).
- 73. G. Ozer, B. Ozbay, Z. C. Oter, G. Tarakci, M. S. Yilmaz, M. E. Bulduk, E. Koc, S. Acar, and K. A. Guler, *Int. J. Cast Met. Res.* **33** (2-3), 146–152 (2020).
- 74. M. Schmid, A. Amado, and K. Wegener, *Proceedings of Pps-30: The 30th International Conference of the Polymer Processing Society*, 2015. p. 1664.
- 75. J. M. Williams, A. Adewunmi, R. M. Schek, C. L. Flanagan, P. H. Krebsbach, S. E. Feinberg, S. J. Hollister, and S. Das, *Biomaterials* **26** (23), 4817–4827 (2005).
- W. Y. Yeong, N. Sudarmadji, H. Y. Yu, C. K. Chua, K. F. Leong, S. S. Venkatraman, Y. C. F. Boey, and L. P. Tan, *Acta Biomater.* 6 (6), 2028–2034 (2010).
- 77. T. B. Bukharova, E. N. Antonov, V. K. Popov, T. K. Fatkhudinov, A. V. Popova, A. V. Volkov, S. A. Bochkova, V. N. Bagratashvili, and D. V. Gol'dshtein, *B Exp. Biol. Med.* **149** (1), 148–153 (2010).
- 78. J. Y. Chen, P. F. Tan, X. J. Liu, W. S. Tey, A. Ong, L. H. Zhao, and K. Zhou, *Virtual Phys. Prototyp.* **17** (2), 295–307 (2022).
- X. Liu, W. S. Tey, J. Y. C. Choo, J. Chen, P. Tan, C. Cai, A. Ong, L. Zhao, and K. Zhou, *Addit. Manuf.* 46, 102205 (2021).
- C. G. Campbell, D. J. Astorga, E. Martinez, and M. Celina, Mrs Commun. 11 (2), 173–178 (2021).
- 81. M. S. Hassan, K. M. M. Billah, S. E. Hall, S. Sepulveda, J. E. Regis, C. Marquez, S. Cordova, J. Whitaker, T. Robison, J. Keating, E. Shafirovich, and Y. R. Lin, *J. Compos. Sci.* **6** (2), (2022).
- 82. C. W. Hull, Apparatus for Production of Three-Dimensional Objects by Stereolithography. United States Patent, Appl., No. 638905, Filed, 1984.
- 83. P. J. Bártolo, *Stereolithography: Materials, Processes and Applications*, Springer Science & Business Media, 2011.
- 84. L. J. Hornbeck, *IEEE Trans. Electron Devices* **30** (5), 539–545 (1983).
- 85. J.-W. Choi, E. MacDonald, and R. Wicker, Int. J. Adv. Manuf. Technol. 49 (5–8), 543–551 (2010).
- C. Sun, N. Fang, D. Wu, and X. Zhang, Sensors Actuators A Phys. 121 (1), 113–120 (2005).

- 87. J. R. Tumbleston, D. Shirvanyants, N. Ermoshkin, R. Janusziewicz, A. R. Johnson, D. Kelly, K. Chen, R. Pinschmidt, J. P. Rolland, A. Ermoshkin, E. T. Samulski, and J. M. DeSimone, *Science* **347** (6228), 1349–1352 (2015).
- 88. X. Kuang, J. Wu, K. Chen, Z. Zhao, Z. Ding, F. Hu, D. Fang, and H. J. Qi, *Sci. Adv.* **5** (5), eaav5790 (2019).
- G. I. Peterson, J. J. Schwartz, D. Zhang, B. M. Weiss, M. A. Ganter, D. W. Storti, and A. J. Boydston, ACS Appl. Mater. Interfaces 8 (42), 29037–29043 (2016).
- X. Peng, L. Yue, S. Liang, S. Montgomery, C. Lu, C. M. Cheng, R. Beyah, R. R. Zhao, and H. J. Qi, Adv. Funct. Mater. 32 (28), 2112329 (2022).
- R. Janusziewicz, J. R. Tumbleston, A. L. Quintanilla, S. J. Mecham, and J. M. DeSimone, *Proc. Natl. Acad. Sci. U. S. A.* 113 (42), 201605271 (2016).
- 92. D. A. Walker, J. L. Hedrick, and C. A. Mirkin, Science 366 (6463), 360-364 (2019).
- 93. D. Martella, S. Nocentini, D. Nuzhdin, C. Parmeggiani, and D. S. Wiersma, *Adv. Mater.* **29** (42), 1704047 (2017).
- 94. D. Yang, L. Liu, Q. Gong, and Y. Li, Macromol. Rapid Commun. 40 (8), 1900041 (2019).
- 95. A. Tudor, C. Delaney, H. Zhang, A. J. Thompson, V. F. Curto, G.-Z. Yang, M. J. Higgins, D. Diamond, and L. Florea, *Mater. Today* 21 (8), 807–816 (2018).
- 96. E.-S. Wu, J. H. Strickler, W. R. Harrell, and W. W. Webb, in *Optical/Laser Microlithog-raphy V*, International Society for Optics and Photonics, 1992.
- S. H. Park, T. W. Lim, D.-Y. Yang, R. H. Kim, and K.-S. Lee, *Macromol. Res.* 14 (5), 559–564 (2006).
- Q. Ge, A. H. Sakhaei, H. Lee, C. K. Dunn, N. X. Fang, and M. L. Dunn, Sci. Rep. 6, 31110 (2016).
- 99. J. J. Schwartz and A. J. Boydston, Nat. Commun. 10 (1), 791 (2019).
- M. Wang, W. Li, L. S. Mille, T. Ching, Z. Luo, G. Tang, C. E. Garciamendez, A. Lesha, M. Hashimoto, and Y. S. Zhang, Adv. Mater. 2107038 (2021).
- Q. Zhang, S. Weng, C. M. Hamel, S. M. Montgomery, J. Wu, X. Kuang, K. Zhou, and H. J. Qi, *Extreme Mech. Lett.* 48, 101403 (2021).
- 102. C. E. Hoyle and C. N. Bowman, Angew. Chem. Int. Edit. 49 (9), 1540–1573 (2010).
- T. Zhao, R. Yu, S. Li, X. Li, Y. Zhang, X. Yang, X. Zhao, C. Wang, Z. Liu, R. Dou, and W. Huang, ACS Appl. Mater. Interfaces 11 (15), 14391–14398 (2019).
- 104. S. C. Lapin, J. R. Snyder, E. V. Sitzmann, D. K. Barnes, and G. D. Green, Stereolithography Using Vinyl Ether-Epoxide Polymers, 1995, Google Patents.
- K. Ohkawa and S. Saito, Resin Composition for Optical Modeling. Patent NumberEP 0360869, 1990.
- R. Yu, X. Yang, Y. Zhang, X. Zhao, X. Wu, T. Zhao, Y. Zhao, and W. Huang, ACS Appl. Mater. Interfaces 9 (2), 1820–1829 (2017).
- X. Kuang, Z. Zhao, K. Chen, D. Fang, G. Kang, and H. J. Qi, *Macromol. Rapid Commun.* 39 (7), 1700809 (2018).
- Z.-X. Zhou, Y.-W. Li, Y.-Q. Zheng, Z. Luo, C.-R. Gong, Y. Xu, and L.-X. Wu, J. Mater. Sci. 54 (7), 5865–5876 (2019).
- J. Herzberger, V. Meenakshisundaram, C. B. Williams, and T. E. Long, ACS Macro Lett. 7 (4), 493–497 (2018).
- M. D. Alim, K. K. Childress, N. J. Baugh, A. M. Martinez, A. Davenport, B. D. Fairbanks, M. K. McBride, B. T. Worrell, J. W. Stansbury, and R. R. McLeod, *Mater. Horiz.* 7 (3), 835–842 (2020).
- 111. S. Deng, J. Wu, M. D. Dickey, Q. Zhao, and T. Xie, Adv. Mater. 31 (39), 1903970 (2019).
- 112. Z. Chen, Z. Li, J. Li, C. Liu, C. Lao, Y. Fu, C. Liu, Y. Li, P. Wang, and Y. He, J. Eur. Ceram. Soc. 39 (4), 661–687 (2019).
- P. Somers, Z. Liang, J. E. Johnson, B. W. Boudouris, L. Pan, and X. Xu, *Light Sci. Appl.* 10 (1), 199 (2021).
- 114. S. K. Saha, D. Wang, V. H. Nguyen, Y. Chang, J. S. Oakdale, and S.-C. Chen, *Science* **366** (6461), 105–109 (2019).

- 115. A. Al Rashid, W. Ahmed, M. Y. Khalid, and M. Koç, Addit. Manuf. 47, 102279 (2021).
- 116. C. Yu, J. Schimelman, P. Wang, K. L. Miller, X. Ma, S. You, J. Guan, B. Sun, W. Zhu, and S. Chen, *Chem. Rev.* **120** (19), 10695–10743 (2020).
- 117. F. Medina, A. Lopes, A. Inamdar, R. Hennessey, J. Palmer, B. Chavez, D. Davis, P. Gallegos, and R. Wicker, *Proceedings of the 2005 Solid Freeform Fabrication*, 2005, pp. 39–49.
- X. Peng, X. Kuang, D. J. Roach, Y. Wang, C. M. Hamel, C. Lu, and H. J. Qi, Addit. Manuf. 40, 101911 (2021).
- D. J. Roach, C. M. Hamel, C. K. Dunn, M. V. Johnson, X. Kuang, and H. J. Qi, Addit. Manuf. 29, 100819 (2019).
- 120. Q. Ge, H. J. Qi, and M. L. Dunn, Appl. Phys. Lett. 103 (13), (2013).
- 121. S. Tibbits, The Emergence of "4D Printing" TED Talks, 2013, Ted Talks.
- 122. Q. Ge, C. K. Dunn, H. J. Qi, and M. L. Dunn, Smart Mater. Struct. 23 (9), (2014).
- 123. X. Kuang, D. J. Roach, J. T. Wu, C. M. Hamel, Z. Ding, T. J. Wang, M. L. Dunn, and H. J. Qi, *Adv. Funct. Mater.* **29** (2), (2019).
- 124. Z. Ding, O. Weeger, H. J. Qi, and M. L. Dunn, Mater. Des. 137, 256–265 (2018).
- 125. B. An, Y. Tao, J. Gu, T. Cheng, X.A. Chen, X. Zhang, W. Zhao, Y. Do, S. Takahashi, and H.-Y. Wu, *Proceedings of the 2018 CHI Conference on Human Factors in Computing Systems*, 2018, ACM.
- D. Han, R. S. Morde, S. Mariani, A. A. La Mattina, E. Vignali, C. Yang, G. Barillaro, and H. Lee, *Adv. Funct. Mater.* 30 (11), 1909197 (2020).
- 127. Kuang, X., D.J. Roach, J. Wu, C.M. Hamel, Z. Ding, T. Wang, M.L. Dunn, and H.J. Qi, Advances in 4D Printing: Materials and Applications. Adv. Funct. Mater., 2018. p. 1805290.
- 128. F. Momeni, S. M. M. Hassani, N. X. Liu, and J. Ni, Mater. Des. 122, 42-79 (2017).
- 129. S. Miao, N. Castro, M. Nowicki, L. Xia, H. Cui, X. Zhou, W. Zhu, S.-J. Lee, K. Sarkar, and G. Vozzi, *Mater. Today* **20** (10), 577–591 (2017).
- 130. M. Shusteff, A. E. Browar, B. E. Kelly, J. Henriksson, T. H. Weisgraber, R. M. Panas, N. X. Fang, and C. M. Spadaccini, *Sci. Adv.* **3** (12), eaao5496 (2017).
- 131. B. E. Kelly, I. Bhattacharya, H. Heidari, M. Shusteff, C. M. Spadaccini, and H. K. Taylor, *Science* **363** (6431), eaau7114 (2019).
- 132. D. Loterie, P. Delrot, and C. Moser, Nat. Commun. 11 (1), 852 (2020).
- M. Regehly, Y. Garmshausen, M. Reuter, N. F. König, E. Israel, D. P. Kelly, C.-Y. Chou,
 K. Koch, B. Asfari, and S. Hecht, *Nature* 588 (7839), 620–624 (2020).
- 134. R. Levato, T. Jungst, R. G. Scheuring, T. Blunk, J. Groll, and J. Malda, *Adv. Mater.* **32** (12), e1906423 (2020).
- X. Liu, H. Yuk, S. Lin, G. A. Parada, T.-C. Tang, E. Tham, C. de la Fuente-Nunez, T. K. Lu, and X. Zhao, Adv. Mater. 30 (4), 1704821 (2018).
- 136. J. Groll, J. A. Burdick, D. W. Cho, B. Derby, M. Gelinsky, S. C. Heilshorn, T. Jüngst, J. Malda, V. A. Mironov, K. Nakayama, A. Ovsianikov, W. Sun, S. Takeuchi, J. J. Yoo, and T. B. F. Woodfield, *Biofabrication* 11 (1), 013001 (2018).
- K. Hölzl, S. Lin, L. Tytgat, S. Van Vlierberghe, L. Gu, and A. Ovsianikov, Biofabrication 8 (3), 032002 (2016).
- M. L. Bedell, A. M. Navara, Y. Du, S. Zhang, and A. G. Mikos, *Chem. Rev.* 120 (19), 10744–10792 (2020).
- R. W. Barrs, J. Jia, S. E. Silver, M. Yost, and Y. Mei, Chem. Rev. 120 (19), 10887–10949 (2020).
- 140. X. Li, B. Liu, B. Pei, J. Chen, D. Zhou, J. Peng, X. Zhang, W. Jia, and T. Xu, Chem. Rev. 120 (19), 10793–10833 (2020).
- 141. U. G. Wegst, H. Bai, E. Saiz, A. P. Tomsia, and R. O. Ritchie, *Nat. Mater.* **14** (1), 23 (2015).
- 142. A. R. Studart, Chem. Soc. Rev. 45 (2), 359–376 (2016).

- 143. Y. Yang, S. Xuan, L. Xiangjia, C. Zeyu, Z. Chi, Z. Qifa, and C. Yong, Adv. Mater. 30 (36), 1706539 (2018).
- 144. Y. Yang, Z. Chen, X. Song, Z. Zhang, J. Zhang, K. K. Shung, Q. Zhou, and Y. Chen, Adv. Mater. 29 (11), 1605750 (2017).
- 145. S. Li, H. Bai, R. F. Shepherd, and H. Zhao, Angew. Chem. 58 (33), 11182–11204 (2019).
- 146. J. J. Martin, B. E. Fiore, and R. M. Erb, Nat. Commun. 6, 8641 (2015).
- 147. V. C.-F. Li, X. Kuang, A. Mulyadi, C. M. Hamel, Y. Deng, and H. J. Qi, Cellulose 26 (6), 3973–3985 (2019).
- 148. G. Siqueira, D. Kokkinis, R. Libanori, M. K. Hausmann, A. S. Gladman, A. Neels, P. Tingaut, T. Zimmermann, J. A. Lewis, and A. R. Studart, Adv. Funct. Mater. 27 (12), 1604619 (2017).
- Q. Shi, K. Yu, X. Kuang, X. Mu, C. K. Dunn, M. L. Dunn, T. Wang, and H. Jerry Qi, Mater. Horiz. 4 (4), 598–607 (2017).
- 150. X. Kuang, D. J. Roach, C. M. Hamel, K. Yu, and H. J. Qi, *Multifunct. mater.* **3** (3), (2020).
- 151. T. Erps, M. Foshey, M. K. Luković, W. Shou, H. H. Goetzke, H. Dietsch, K. Stoll, B. V. Vacano, and W. Matusik, *Sci. Adv.* 7 (42), eabf7435 (2021).
- K. Maute, A. Tkachuk, J. Wu, H. J. Qi, Z. Ding, and M. L. Dunn, J. Mech. Des. 137 (11), 111402 (2015).
- 153. E. Salvati and A. Korsunsky, Int. J. Mech. Sci. 138, 457–466 (2018).
- S. M. Montgomery, C. M. Hamel, J. Skovran, and H. J. Qi, *Extreme Mech. Lett.* 53, 101714 (2022).
- 155. Z. Zhu, S.-Z. Guo, T. Hirdler, C. Eide, X. Fan, J. Tolar, and M. C. McAlpine, *Adv. Mater.* **30** (23), 1707495 (2018).
- H. Craig, R. Devin, L. Kevin, D. Frederic, D. Martin, and Q. Jerry, *Smart Mater. Struct.* 28, 065005 (2019).
- 157. S. Wu, C. M. Hamel, Q. Ze, F. Yang, H. J. Qi, and R. Zhao, *Adv. Intell. Syst.* **2** (8), 2000060 (2020).
- 158. X. Sun, L. Yue, L. Yu, H. Shao, X. Peng, K. Zhou, F. Demoly, R. Zhao, and H. J. Qi, *Adv. Funct. Mater.* **32** (10), 2109805 (2022).

XIAO KUANG H. JERRY QI School of Mechanica

School of Mechanical Engineering Georgia Institute of Technology Atlanta, GA, USA

Wei Shian Tey

HP-NTU Digital Manufacturing Corporate Lab, School of Mechanical and Aerospace Engineering Nanyang Technological University Singapore, Singapore

Kun Zhou

HP-NTU Digital Manufacturing Corporate Lab, School of Mechanical and Aerospace Engineering Nanyang Technological University Singapore, Singapore Singapore Centre for 3D Printing, School of Mechanical and Aerospace Engineering Nanyang Technological University Singapore, Singapore